This pre-print has been submitted in 2019 to the Geological Society of London Special Publication on Subaqueous Mass Movements and Their Consequences. It has undergone peer review and is subject to change during the proof preparation and typesetting stage.

The Last Glacial Maximum Balearic Abyssal Plain Megabed revisited

Antonio Cattaneo[1*], Shray Badhani[1,2] Cristina Caradonna[3], Massimo Bellucci[2,3], Estelle Leroux[1], Nathalie Babonneau[2], Sébastien Garziglia[1], Jeffrey Poort[4], Grigorii G. Akhmanov[5], Germain Bayon[1], Bernard Dennielou[1], Gwenael Jouet[1], Sebastien Migeon[6], Marina Rabineau[2] Laurence Droz[2] & Michael Clare[7]

[1]*IFREMER, Géosciences Marines, Plouzané, France*
[2]*UMR 6538 Géosciences Océan, Université de Brest, France*
[3]*Università di Trieste, Italy* km^2
[4] *UMR 7193 ISTeP, Sorbonne Université, Paris, France*
[5] *Lomonosov Moscow State University, Moscow, Russian Federation*
[6] *UMR7329, GEOAZUR, Valbonne, France*
[7] *National Oceanography Centre, University of Southampton, United Kingdom*
**Corresponding author (e-mail: antonio.cattaneo@ifremer.fr)*

Abstract: Megabeds are thick sedimentary layers extending over thousands square kilometres in deep sea basins and are thought to result from large slope failures triggered by major external events. Such deposits have been found in at least three areas of the Mediterranean Sea. Although their discovery dates back to the early 1980s, many questions remain, concerning their initiation, source area, extent, and the nature of their emplacement. One of the largest previously documented megabeds was emplaced during the Last Glacial Maximum across the Balearic Abyssal Plain with a thickness of 8-10 m in water depths of up to 2800 m.

New 3.5 kHz sub-bottom profiles and sediment cores provide greater constraint on the lateral variability of the megabed and allow to map it beyond previous estimates, with a revised areal extent up to 90,000-100,000 km^2. Megabed terminations show gradual pinch-out to the West and an abrupt eastward termination against the Sardinia steep margin. The megabed presents both in seismic profiles and in sediment cores a tripartite subdivision likely corresponding to changes in flow regimes across the basin with a central area of sandy facies and erosional base oriented NNE-SSW allowing renewed discussions about sources and trigger of the megabed.

1. Introduction

Anomalously thick (up to some 10s of m) acoustically transparent sedimentary layers known as megabeds or megaturbidites are found in at least three deep basins of the Mediterranean Sea: the Balearic Abyssal Plain (Rothwell et al., 1998); the Ionian Sea (Cita and Aloisi, 2000, Hieke et al., 2003) and the Herodotus basin in the eastern

Mediterranean (Reeder et al. 2000). These deposits have volumes equivalent to some of the largest mass movements documented worldwide, often in excess of 100 km^3 (Fildes, 2013 and references therein). The term megaturbidite indicates a turbidite (that is a fining upward sand/silt/clay bed accumulated from a waning turbulent semi-laden flow; Mutti, 1992) whose thickness is larger than the average surrounding turbidite beds above and below, that has a peculiar composition and basinwide extent (Bouma, 1987). Typically, megabeds are recognized in abyssal plain settings. In some cases, megabeds are capped by a thick (pluri-metric) accumulation of dominantly structureless, homogeneous silty clay without microfossil content also referred to as homogenite (Kastens and Cita, 1981; Cita et al., 1984). In this study we use the term 'megabed', because the terms 'megaturbidite' and 'homogenite', though describing sedimentary facies, are also genetically connoted and correspond to the HmTu couplet of genetically linked deposits (e.g. Campos et al., 2013). The reason to study megabeds is twofold. Firstly, in spite of their massive appearance, scarce detailed information on sedimentary structures is available in the literature, which has inhibited a clear interpretation of the associated sedimentary processes at the origin of these anomalously large event deposits. Secondly, they may be diagnostic of major catastrophic events as their triggering is usually attributed to major external events, including large earthquakes and tsunamis, or may themselves have triggered tsunamis (e.g., Talling et al., 2014). The emplacement of such a megabed could impact important deep-sea benthic communities as a result of widespread and rapid burial of the seafloor over hundreds of square kilometres, as well as the prolonged (>>months) effects of turbid waters during the settling of suspended fine sediments. Following the 12 January 2010 Haiti Mw 7.0 earthquake, a 600-m thick nepheloid layer took two months to settle after the initial event (McHugh et al., 2011).

As megabeds typically form widespread, low-relief deposits that blanket broad basin topography, their identification from seafloor data is challenging. As a result, their identification is usually based on the recognition of extensive acoustically transparent layers in sub-bottom profiles, a diagnostic echo-facies signature that results from the generally homogenous nature of the deposits (Damuth, 1980; Cita et al., 1984). Several hypotheses have been proposed concerning their mechanisms of origin all associated with catastrophic high magnitude events (e.g. volcanic activity, earthquakes, tsunamis). Recent studies have proposed scenarios where multiple sedimentary processes contribute to the emplacement of megabeds (e.g., Mulder et

al., 2009; SanPedro et al., 2017) or have resulted in the revision of previous age estimates for event timing. For instance, more accurate age dating linked the Augias megabed in the Ionian Sea to the large historical earthquake of 365 AD in the island of Crete (Vigliotti et al., 2006; Polonia et al., 2013; SanPedro et al., 2017), rather than the previously-assumed trigger, which was inferred to be the Santorini volcanic eruption (3500 BP; Cita et al., 1984). Given their prodigious volumes, it is remarkable that there are still so many unanswered questions about the nature and processes related to these megabeds.

Although the discovery of megabeds dates back to the early 1980s (Kastens and Cita, 1981), there are open questions concerning megabeds about: (1) determining precise recurrence times of these deposits when present in superimposed layers, with important implication for the reconstruction of past catastrophic events; (2) the physical and mechanical characteristics of these deposits for more strictly constraining the sedimentary processes that resulted in these exceptional sediment accumulation events and their impact on benthic communities; (3) the sedimentary and geochemical sources of the sediment forming the megabeds. The Balearic Abyssal Plain (BAP) megabed, the largest megabed in the Mediterranean, is a perfect example of a puzzling deposit. While its age is well constrained by multiple radiocarbon dates and biostratigraphy (Rothwell et al., 1998; Hoogakker et al., 2004), the initiation processes and source areas remain far from clear; even on a regional basis (Rothwell et al., 1998; 2000; Droz et al., 2006). It is remarkable that a deposit with an estimated volume of 500-600 km^3 has no obvious source, especially given the extent of marine geological studies around the western Mediterranean in recent years (e.g., Dennielou et al., 2019; Badhani et al., 2019). In order to understand the hazard posed by these large sediment transport events, it is important to address these uncertainties. Where did they come from? How did they initiate? What is their full spatial extent? What process(es) explain their emplacement and are multiple phases of activity involved? These questions are particularly important given the dense coastal populations that border confined Mediterranean basins, such as the Balearic Abyssal Plain, and as megabed emplacement is not a one-off event in these settings. Stacked megabeds have been observed in seismic data, indicating that these are recurrent events both in Quaternary sediment (e.g. in the Ionian abyssal plain, Heike et al., 2002; in the Marmara Sea, Beck et al., 2007) and in ancient deposits (e.g. Amy and Talling, 2006 in the Northern Apennines; Fallgatter et al., 2016 in Argentina).

Sub-bottom seismic profiles are an important data set for near-surface structural and sedimentological analysis. This is why we present a basin-wide analysis of the newly available sub-bottom profile data and a comparison with, in part, already published analysis of sediment cores sampling the BAP megabed. We present an extensive (though not comprehensive, as the vast area of the BAP is scarcely covered by geophysical surveys, see **Fig. 1**) view of the geometry, terminations, bounding surfaces and internal geometries of the megabed. We also set up the first steps for a match of seismic to core data to reconstruct the sedimentary processes at the origin of the megabed based on integrated and complementary new evidences. The aim of this study is to highlight details in the seismic images of the BAP megabed that unveils aspects of the sedimentary processes at its origin and source: in particular we present detailed diagnostic features of sedimentary processes including evidence of localised basal erosion, considerations on the nature and internal variability of the megabed indicative of possible flow transformations, and some results on the mechanical properties of the homogenite part.

2. Background

The Western Mediterranean Basin formed behind a Miocene volcanic arc with the clockwise rotation of the Corsica-Sardinia block and the opening of the Provencal Basin (Rehault et al., 1984). It is the youngest part of the Mediterranean formed from late Oligocene to present (Mauffret et al., 2004). The BAP is the largest abyssal plain of the Mediterranean with an area of about 77,000 km^2 and may be identified by the 2800-m isobath (Rothwell et al., 1998, 2000). It is surrounded by passive margins of the Gulf of Lions and Ligurian Sea with the Rhone and Var fans to the north, by the Algerian margin to the south, by the Balearic margin and the Valencia fan to the west, and by the Sardinian-Corsican margin to the east, with continental shelves variable from the 200-km wide Gulf of Lions to less than 50 km along Corsica, Sardinia and north Africa (Rothwell et al., 1998; Hoogakker et al., 2004; Zuniga et al., 2007). Sources for turbidity currents have been documented from several of these continental margins and include earthquake triggered events associated with tsunami waves, such as the 2003 Boumerdès event (Cattaneo et al., 2012).

The most striking morphological feature of the BAP is the presence of a thick Messinian evaporite layer, salt walls and diapirs at the seafloor (Stanley et al., 1974). Another key feature of the BAP is a thick layer identified in the abyssal plain by its acoustically

transparent signature in sub-bottom profiles, called “megaturbidite” (Rothwell et al., 1998), which extends over the whole extent of the abyssal plain and reaches a thickness of 8–10 m in the centre of the basin (Rothwell et al., 1998, 2000). The longest core records of the BAP megabed are the giant Calypso piston cores recovered during the campaign PALAEOFLUX in 1995 (Rothwell and Balut, 1995; Tab. 1). These piston cores, up to 32 m in length, were recovered along a SSW-NNE transect, were located about 120 km apart from each other (**Fig. 1**), and were dated to reconstruct the stratigraphic history of the accumulation that accounts for up to 150 kyr and is constituted by about 90% of turbiditic successions and only 10% of hemipelagites (Rothwell et al., 2000; 2006; Hoogakker et al., 2004; Clare et al., 2014). Turbidite bases towards the northern part of the BAP are thicker and coarser in grain size, indicating a more likely provenance from the north according to Hoogakker et al. (2004). The attribution of the age of the megabed is based on 10 radiocarbon ages above and below the megabed in cores MD95-LC01, -LCO2, -LC04, -LC05 and -LC06 (Rothwell et al., 1998). Dennielou et al. (2019) performed a recalibration of the five dates on top of the megabed following Reimer et al. (2013) and obtained a 2-sigma age comprised between 20.3 and 20.9 ka cal BP with a median probability of 20.6 ka cal BP, within the Last Glacial Maximum.

3. Data and methods

3.1 Sub-bottom profiles

All available sub-bottom data within the interest area were integrated in a single Kingdom database for interpretation. This includes in particular the newly acquired data during the WestMedFlux survey (Poort and Lucazeau, 2016; Poort and Gorini, 2018; **Figs 2-5**), but also the datasets from the PROGRES (Droz, 2003) and SARDINIA (Aslanian and Olivet, 2006) campaigns. Some profiles from AM-MED (Rabineau et al., 2013) survey were also integrated. Successive processing steps were applied onboard consisting of correlation (signal compression), correction of the spherical divergence, compensation of the ship movements (pitch, roll and heave), calculation of the location of the source and receptors, and correction for the delay. Imports of sub-bottom data in Kingdom were applied in amplitude, and envelope was computed for each segy file. Locations of cores were also loaded into the database to be correlated with the seismic data (**Tab. 1**).

3.2 Sediment cores

Sediment cores reaching the top or the entire BAP megabed are summarised in **Table 1**, including cores presented in the literature and in this study (**Figs. 6, 7**). In most cases, the identification of the BAP megabed is based on two criteria for cores in the central part of the abyssal plain: 1) the identification of a turbidite layer outpacing in thickness the encasing successions of alternating hemipelagites and thin bedded turbidites, and 2) the attribution to a comparable age range as that reported by Rothwell et al. (1998) recalibrated by Dennielou et al. 2019). Grey homogeneous mud beds identified in cores PSM-KS21 (~8.8 m bsf – below seafloor), PSM-KS23 (~5 m bsf) and PSM-KS27 (~11 m bsf) are correlated to the BAP megabed mainly based on age attribution (**Tab. 2**), but also on sedimentary facies characters, mainly the sediment colour different from adjacent beds and the homogeneous structureless texture (**Fig. 8**).

Sediment core WMF2-KF11 is positioned on seismic profile WMF2016-AT006 by adopting a velocity of 1529 m s^{-1} based on an averaged value of the Multi Sensor Core Logger data (P-wave velocity) measured on the whole core (**Fig. 6**). Radiocarbon dates on core WMF2-KF11 were obtained by AMS at Beta Analytic laboratory and calibrated with MARINE 13 database (Reimer et al., 2013) (**Tab. 2**).

Geotechnical analyses were performed on core WMF2-KF11 (**Fig. 9**). They included measurements on freshly open core (water content, vane shear, P-wave velocity with a celerimeter). Four oedometer tests were performed on samples from the same core, two within the megabed, two in overlying sediments. Values of compressional wave velocities, undrained shear strength (peak and residual) and water content were measured on split sections of core WMF2-KF11 using devices and approaches as reported in Miramontes et al., (2018). Four oedometer tests with incremental loading were also carried out on preserved samples from the same core to determine the recompression (Cr), compression (Cc) and swelling indices (Cs) as well as the yield stress ratio (YSR) of sediments.

4. Results

4.1 Expression and variability of the BAP megabed in sub-bottom profiles

With the available bathymetric and seismic reflection dataset it is difficult to have an exhaustive view of all the lateral variability of the BAP megabed due to the lack of complete coverage of the abyssal plain. The BAP is characterised by variable

morphologies and structures linked to halokinesis of Messinian evaporites creating a highly variable seafloor landscape. To account for such variability we present here some evidence of the expression of the megabed in distinct sectors of the abyssal plain, including megabed terminations (**Fig. 3**), erosion at the base of the megabed (**Fig. 4**) and internal subdivisions (**Figs. 5-7**). The BAP megabed is identifiable as an acoustically transparent layer all over the area outlined by a black line in **Figure 1** and corresponding to the limits of this layer according to Rothwell et al. (1998, 2000), that is to the 2800 m isobath. Sub-bottom profile WMF2016-AT010 shows the laterally continuous acoustically transparent unit of the BAP megabed less than 10 m below the seafloor, with gentle folds following the geometry of underlying strata and a gradual pinch-out of the unit towards the west (**Fig. 2a**). In sub-bottom profile WMF2018-AT141A, however, the same acoustically transparent layer presents still a good degree of lateral continuity, but with accentuated effect of deformation due to the presence of salt domes: it is also possible to lose the lateral continuity of the layer and find it beyond the highest salt domes (see **Fig. 3a** towards the west). In **Figure 2b** sub-bottom profile WMF2016-AT shows towards the east, in the central part of the basin, the presence of faults, likely linked to salt dome movements, displacing the megabed of several metres either in distinct locations (**Fig.2b**, towards the west) or in sets of narrowly spaced faults (**Fig. 2b**, towards the east). By appreciating the geometry of the BAP megabed and that of the underlying strata, it is possible to deduce that the halokinetic deformation postdates the emplacement of the megabed.

Another characteristic feature of sedimentary bodies, and of their expression as seismic units, is the geometry of pinch-out terminations. Two constrasting styles of megabed termination exist on two opposite sides of the abyssal plain (**Fig. 3**). Towards the West, the pinch-out of the BAP megabed seems to be at offset 15000, but it actually goes gradually further west beyond an area with salt dome (offset 1000 in **Fig. 3a**). Towards the east, the termination of the acoustically transparent unit is against the Sardinia margin, which is relatively steep with a slope angle exceeding 11° (Deiana et al., 2016). The termination is abrupt, passing from about 10 ms in thickness to zero, masked by the hyperbolae of the Sardinian margin (**Fig. 3b, c**). In this latter case the termination reminds of the first identifications of ‘homogenites’ in the Eastern Mediterranean by Kasten and Cita (1981), who described these deposits as flat-lying within each basin where they deposit with abrupt terminations against the steep basin walls. The megabed thickness is not thinning gradually towards the West, but presents

values increasing irregularly towards the centre of the basin also due to deformation by salt domes (**Fig. 3b**).

The contact of the megabed with the underlying strata is conformable in the majority of the analysed seismic lines (**Figs. 2, 6**), but, especially in the central area of the BAP, the contact is irregular (**Fig. 4**). A diagnostic indicator of the processes generating turbidite beds is the nature of the beds basal surfaces in being erosional. **Figure 4 (a, b)** presents evidence of seismic reflectors truncated below the base of the megabed: we interpret these features,present mostly in the area comprised within a dashed blue line in **Figure 4c**, as localised erosional features. An alternative interpretation might suggest that these features have resulted from fluid escape, but this is highly unlikely, because of the lack of evidence in this sector of vertical anomalies in the seismic profiles that could be identified as fluid escape chimneys. Other sub-bottom profiles in this central-western area of the abyssal plain show similar features.

Far from being fully homogeneous, the dominantly acoustically transparent megabed presents also a certain variability in its acoustic response. We summarise this variability in three slightly differentiated seismic echo-facies (Damuth et al., 1980; (**Fig. 5)**. Echo-facies I, below the top of the megabed, presents faint discontinous and very low amplitude reflectors. Echo-facies II is dominantly transparent, but it is topped by a discontinuous seismic reflector mappable in several areas where the megabed is relatively thick. Finally, Echo-facies III is characterised by a discontinuous base and top showing medium-amplitude discontinuous reflectors: it also occurs in association with local erosional features (**Fig. 4b**). Echo-facies III is present at the base of the megabed where it reaches a thickness exceeding ca. 10 ms in the central area of the abyssal plain (**Fig. 4c)**. The three echo-facies cannot be identified thoroughly over the entire extent of the megabed.

4.2 Sediment character of the BAP megabed

Lithology and sedimentary structures of the BAP megabed known from the literature are compared with new observations on core WMF2-KF11. **Table 1** shows the identification of the BAP megabed its grain size divisions and their depth in 10 cores: five MD81 cores published in Rothwell et al. (1998), three PSM cores presented in Babonneau et al. (2017) and two WMF2 cores presented here (Poort and Gorini, 2018). The presesence of the BAP megabed is also suggested in two additional WMF cores (Poort and Lucazeau, 2016). In general, cores located within the limits identified

by Rothwell et al. (1998) and reaching the megabed present an overall bipartite lithology with a normally graded sandy to silty base capped by a homogeneous clay unit that can be several metres thick. The megabed can thus be described as a *HmTu* couplet, since it is composed of two distinct components (Campos et al., 2013; see also McHugh et al. 2006).

Sediment core WMF2-KF11 was collected at 2848 m water depth in the central part of the Balearic abyssal plain. It is 5.92 m long and presents brownish yellow silty clay with foraminifera and shell fragments in the upper ca 30 cm, gradually passing to alternating very thin to medium thick normally graded sandstones and olive grey silty clays down to 2.28 metres below sea floor (mbsf; **Figs. 6b,d, 7**). This interval is interpreted as alternating turbidites and hemipelagites. The rest of the core down to 5.92 mbsf is composed of homogeneous dark grey silty clay (2.28 to 4.50 mbsf), dark grey clayey silt with sub-millimetric laminae (4.50 to 5.25 mbsf), and dark grey structureless, possibly normally graded silt. The entire interval from 2.28 to 5.92 mbsf is interpreted as part of the BAP megabed including the *Hm* division (2.28-4.50 mbsf) and part of the *Tu* division (*sensu* Campos et al., 2013). By using a conversion velocity of 1529 m s^{-1} based on MSCL data **(Fig. 6c)**, the core is projected on the sub-bottom profile WMF2016-AT006 (**Fig. 6a**). It is possible to tentatively correlate the three echo-facies to sedimentary facies: echo-facies I would correspond to sandy turbidite facies, echo-facies II to silty turbidite, and echo-facies III to homogenite.

The same tripartition of sedimentary facies within the megabed in core WMF2-KF11 is visible also in core LC05 which is in the southwestern sector of the BAP (**Fig. 7**). The megabed presents a sharp and irregular (eroded) base and a upper gradational and bioturbated contact. Its grain size is coarse sand to clay with positive grading, although negative grading may exist in the coarse fraction at the base. There is an overall upward fining trend to the homogeneous mud unit at the top, with a slight grain size break at the transition from silt to mud (**Fig. 7b**). The sedimentary structures include a mostly massive basal division with faint planar lamination which may include planar intra-bed contacts at the base and a transition into cross-bedded, climbing ripples and convolute laminae (**Fig. 7b**).

The megabed likely represents a ponded megaturbidite resulting from steady long-lived turbidity current as suggested in the existing literature (e.g., Rothwell et al., 1998, 2000; Clare et al., 2014). Planar laminae formed as a result of grain flow at the turbidity

current head. The rest of the flow settled out due to low density turbulent suspension and/or gel strength and/or excess pore pressure.

A transect of sediment cores offshore the Algerian margin (PSM3-KS21, PSM3-KS23 and PSM3-KS27; **Fig. 8**) fully described in Babonneau et al. (2017; their Fig. 7) shows a sedimentary succession of fining-upward sandy/silty layers (turbidites) alternating with thin mud layers (hemipelagites). A mud layer stands out in photos for its grey colour different from that of other encasing layers. The age constraint above and below the grey bed (Babonneau et al., 2017; **Tab. 2**) suggests that it is possible to identify it as the distal expression of the BAP megabed. This Identification of the BAP megabed in distal cores goes up to 200 km beyond the pinch-out of the megabed as visible in seimic lines and suggests that also other cores, such as for example cores WMF-KF10 and -KF11 south of the Balearic Islands could contain the same layer (**Fig. 1**; **Tab. 1**).

4.3 Mechanical properties of the BAP megabed in core WMF2-KF11

A marked change in both density and Vp profiles occurs at 2.28 m (**Fig. 9**). This change is reflected by Yield Stress Ratios (YSR) higher than 1 above 2.28 m and lower than 1 below. However, except the recompression indices, the other indices determined from oedometer tests do not show a clear change; this contrasts with the values of undrained shear strength (Su) which decrease abruptly below 2.28 m (**Fig. 9**). Comparisons with the trends generally exhibited by normally consolidated sediments (Su= 0.2 σ'v or 0.3 σ'v; e.g., Garziglia et al., 2010) can be reconciled with YSR values to indicate that below 2.28 m the sediment is under-consolidated.

5. Discussion

5.1 Overall distribution of the BAP megabed and inference on sources

The BAP megabed is reported in the literature as extending in the BAP identified by the isobath 2800 m over a surface of 60,000 km^2 for a volume of 500 km^3 (Rothwell et al., 1998), and, successively, over a surface of 77,000 km^2 for a volume of 600 km^3 (Rothwell et al., 2000; Hoogakker et al., 2004). We find, thanks to the identification of a distal correlative of the megabed to the West (**Fig. 8**), that the megabed extends 200 km further along the central Algerian basin (**Fig. 1**, dashed lines). The resulting extent would thus become of up to 90,000-100,000 km^2, while the total volume would not be much affected by this extension and would become of up to 640 km^3, because of the limited thickness of this part of the megabed (< 1 m; **Fig. 8**).

Beyond its considerable size, the importance of the information coming from the analysis of the BAP megabed consist in its exceptional state of preservation and basinwide extent. The BAP megabed has preserved much detail that is missing in many other more ancient settings, but unfortunately the extent of the dataset is limited and uneven. Core data (**Tab. 1**) show that the distribution of the megabed thickness has a maximum in the deepest central part of the BAP (core LC04). The contrasting style of megabed terminations with a gradual pinch-out towards the West and an abrupt termination with more important thickness to the East could be related to the distance from the source, but also to an enhanced effect of ponding, or, rather, possibly oblique reflection against the steep Sardinia margin (*sensu* Kneller et al., 1991).

As in the case of several ancient megabeds in outcrops, the provenance problem cannot simply be solved by a single argument. The sediment provenance of the Oligocene Numidian megabed is debated and attributed to European sources based on zircon analysis (Fildes et al., 2010) to African provenance (Thomas et al., 2010) or again African based on a series of argumentations including paleogeographic reconstructions (Stow et al. 2010). The case of the BAP megabed could be theoretically simpler, because paleogeography during the Last Glacial Maximum can be inferred with a higher degree of certainty and basically corresponds to the present one with a sea level lowered of about 120 m during the Last Glacial Maximum (**Fig. 7c** modified from Clare et al., 2014). Nevertheless, the solution is not easy and several independent lines of evidence have to be explored, possibly with the support of future geochemical investigations. The location of historical seismicity, concentrated in three sectors (Ligurian, Pyrenean and Algerian margins) could suggest possible source areas of mobilised sediment following major earthquakes (**Fig. 7c**).

5.2 Internal structure of BAP megabed and inferred sedimentary processes

Hoogakker et al. (2004) and Rothwell et al. (2006) found that over the last 130 kyr over 90% of the sediment accumulation in the BAP was composed of turbidites and that the overall amount of erosion was negligible, allowing a rather continuous record of hemipelagites. By analysing in detail Sub-Bottom profiles, we found that the base of the BAP megabed could be in part an exception to this general rule, and we think that this fact could be interesting for sedimentary processes reconstructions. Even if the interpretation of erosional base of turbidite beds is far from being straightforward (Eggenhuisen et al., 2011), the evidence of seismic reflector truncations and in

particular the location of zones of enhanced basal erosion could suggest areas of the BAP impacted by stronger turbidity flows in the center of the BAP (**Fig. 4**). The distribution of the erosional areas in available profiles suggests that the area of erosion is oriented along a roughly N-S or NE-SW orientation; it is possible that this orientation represents a direction of axial transport of the main initial flow in the deepest part of the basin.

The notion of turbidity currents running very long distances down to the abyssal plains has been demonstrated in several cases both in recent and ancient case studies (e.g., Zuffa et al., 2000; Clare et al., 2014). Zuniga et al. (2007) demonstrated that turbidity currents originated from continental margins surrounding the BAP can reach the centre of the basin during sea level highstands as the present one. An implication in the long distance of a turbiditic flow is the series of flow transformations that could occur along the turbidity flow path (Haughton et al., 2009; Talling, 2013; Fallgatter et al., 2016). The tripartite structure of the megabed found in seismic profiles and in sediment cores might reflect flow transformations, even if, given the scarce spatial coverage of the data it is difficult to reconstruct a continuous scenario of flow evolution. We agree with former interpretations of sediment cores (e.g., Rothwell et al., 2000; Clare et al., 2014) considering the megabed as a single event and we think that the presence/absence of tripartition in echo-facies could be due to changes in flow velocity possibly linked to seafloor irregularities such as the presence of salt domes.

Finally, the homogenite shows peculiar physical and geotechnical properties, in particular the consolidation state (underconsolidated). The megabed appears to be composed of sediment which remained under-consolidated since its deposition. Water incorporation during the flow may explain the under-consolidated state of the sediments during tens of years after rapid deposition. However, since burial has ensued over the last ca. 20 kyr, one might expect this characteristic signature to have been erased upon consolidation unless the transport and depositional process gave the deposit an atypical structure (combination of particle arrangement and bounding). This underconsolidation could be suggestive of extremely rapid and water-saturated deposition of the megabed with the clay on top acting as a seal and could further support the hypothesis of a relatively rapid accumulation from a single event. In situ tests such as CPTU (cone penetration test undrained with measurement of excess pore pressure) could thus help confirm this observation.

6. Conclusions

A large deposit sitting on the Balearic Abyssal Plain - originally mapped by using the extent of acoustically transparent reflection - has been redefined and remapped to discover that it is larger than previously thought. The Balearic Plain megabed is one of the most known examples of megabeds in abyssal plains and an analogue to megabeds studied in outcrop of ancient rocks. It occupies the whole abyssal plain over an extent of at least 77,000 km^2, but up to 90,000-100,000 km^2 and with a thickness of 8-10 m in the centre of the basin and a volume of up to 640 km^3, comparable to giant landslide deposits. The megabed is affected by faults and halokinetic deformation (salt domes) suggesting recent (post LGM) activity of tectonics based on the age of the deformed megabed.

The internal geometry of the BAP megabed presents three faint but distinctive echo-facies from bottom to top that correspond tentatively to the three sedimentary faces identified in cores possibly linked to flow transformations within a single event bed. The analysis of new data in the area allowed to present some details of its geophysical appearance, in particular the presence of contrasting pinch-outs on the abrupt eastern Sardinian margin, whereas the limit is asymptotal towards the West. This suggests that there could have been some reflected turbidite pattern against the Sardinia margin.

In the central area of the abyssal plain, the basal layer of the BAP megabed shows evidence or erosional truncation of underlying deposits that might indicate enhanced erosion of turbiditic flows and/or proximity of sedimentary sources: however a composite source from several margins cannot be discarded at the present state of knowledge. Further work on geochemistry of the sediment cores could help identify the source areas and thus the geographic location of predisposing mechanisms that influenced the deposition of the Western Mediterranean megabed, and enhance the understanding of geohazard in the Mediterranean region.

Acknowledgements

We thank the captains, crew and science parties of campaigns WESTMEDFLUX (R/V L'Atalante 2016, 2018, DOI:10.17600/16000600), AM-MED (R/V Le Suroit, 2013, DOI:10.17600/13020050 PRISME (R/V L'Atalante 2007, DOI:10.17600/7010090), SARDINIA (R/V L'Atalante, 2006, DOI:10.17600/6010150), PROGRES (R/V Le Suroit 2003, DOI:10.17600/3020080). We thank core repositories BOSCORF (NOC,

Southampton, UK) and CREAM (IFREMER, Géosciences Marines, Brest, France) and their staff for support in core maintenance/handling and assistance in analytical techniques. This project has received funding from the European Union's Horizon 2020 research and innovation programme under the Marie Skłodowska-Curie grant agreement No 721403 (ITN SLATE project, PhD of S Badhani). This contribution would not have been possible without the precious suggestions and encouragements of Reviewers C. McHugh and A. Fildani, and without the scientific guidance and perseverance of Guest Editor A. Georgiopoulous.

References

Amy, L.A. & Talling, P. 2006. Anatomy of turbidites and linked debrites based on long distance (120-30 km) bed correlation, Marnoso Arenacea Formation, Northern Apennines, Italy. Sedimentology, **53**, 161-212.

Aslanian, D. & Olivet, J.L. 2006. SARDINIA cruise, RV L'Atalante, https://doi.org/10.17600/6010150

Babonneau, N., Cattaneo, A., Ratzov, G., Déverchère, J., Yelles-Chaouche, A., Lateb, T. & Si Bachir, R. 2017. Turbidite chronostratigraphy off Algiers, central Algerian margin: A key for reconstructing Holocene paleoearthquake cycles. *Marine Geology*, **384**, 63-80. https://doi.org/10.1016/j.margeo.2016.10.017

Badhani, S., Cattaneo, A., Dennielou, B., Leroux, E., Colin, F., Thomas, Y., Jouet, G., Rabineau, M. & Droz, L. 2019. Morphology of retrogressive failures in the Eastern Rhône Interfluve during the Last Glacial Maximum (Gulf of Lions, Western Mediterranean). *Geomorphology*. in press. doi.org/10.1016/j.geomorph.2019. 106894

Beck, C., Mercier de Lépinay, B., Schneider, J.-L., Cremer, M., Cagatay, N. Wendenbaum, E., Boutareaud, S., Ménot, G., Schmidt, S., Weber, O., Eris, K., RArmijo, R., Meyer, B., Pondard, N., Gutscher, M-A., and the MARMACORE Cruise Party 2007. Late Quaternary co-seismic sedimentation in the Sea of Marmara's deep basins. *Sedimentary Geology*, **199**, 69-85. 10.1016/j.sedgeo.2005.12.031 .

Bouma, A.H. 1987. Megaturbidite: an acceptable term? *Geo Marine Letters*, **7**, 63-67.

Campos C., Beck, C., Crouzet, C., Carrillo, E., Van Welden, A. & Tripsanas, E. 2013. Late Quaternary paleoseismic sedimentary archive from deep central Gulf of Corinth: time distribution of inferred earthquake-induced layers. *Annals of Geophysics,* **56**, 6, S0670; doi:10.4401/ag-6226.

Cattaneo, A., Babonneau, N., Ratzov, G., Dan-Unterseh, G., Yelles, K., Bracène, R., Mercier de Lépinay, B., Boudiaf, A. & Déverchère, J. 2012. Searching for the seafloor signature of the 21 May 2003 Boumerdès earthquake offshore central Algeria. *Natural Hazard and Earth System Sciences*, **12**, 2159-2172. Publisher's official version : http://dx.doi.org/10.5194/nhess-12-2159-2012

Cita, M.B. & Aloisi, G. 2000. Deep-sea tsunami deposits triggered by the explosion of Santorini (3500 y BP), eastern Mediterranean. *Sedimentary Geology*, **135**, 181-203.

Cita, M.B., Camerlenghi, A., Kastens, K.A. & McCoy, F.W. 1984. New findings of bronze age homogenites in the Ionian Sea: geodynamic implications for the mediterranean. *Mar. Geol*. **55**, 47-62.

Clare, M.A., Talling, P.J., Challenor, P., Malgesini, G. & Hunt, J. 2014. Distal turbidites reveal a common distribution for large (> 0.1 km^3) submarine landslide recurrence. *Geology*, **42**, 263-266. https://doi.org/10.1130/G35160.1

Damuth, J.E.D. 1980. Use of high-frequency (3.5-12 kHz) echograms in the study of near-bottom sedimentation processes in the deep-sea: A review. *Marine Geology*, **38**, 51-75. DOI: 10.1016/0025-3227(80)90051-1

Deiana, G., Meleddu, A., Paliaga, E.M., Todde, S. & Orrù, P.E. 2016. Continental slope geomorphology : landslides and pockforms of Southern Sardinian margin (Italy). *Geogr. Fis. Dinam. Quat*. **39**, 129-136. DOI 10.4461/GFDQ.2016.39.12

Dennielou, B., Jégou,I., Droz, L., Jouet, G., Cattaneo, A., Berné, S., Aslanian, D., Loubrieu, B., Rabineau, M. & Bermell, S. 2019. Major modification of sediment routing by a large Mass Transport Deposit in the Gulf of Lions (Western Mediterranean). *Marine Geology*, **411**, 1-20. https://doi.org/10.1016/j.margeo. 2019.01.011

Droz, L., 2003. PROGRES cruise, RV Le Suroît, https://doi.org/10.17600/3020080

Droz, L., dos Reis A.T., Rabineau, M., Berné, S. & Bellaiche, G. 2006. Quaternary turbidite systems on the northern margins of the Balearic Basin (Western Mediterranean): a synthesis. *Geo-Marine Letters,* **26**, 347-359.

Eggenhuisen, J.T., McCaffrey, W.D., Haughton, P.D.W. & Butler, R.W.H. 2011. Shallow erosion beneath turbidity currents and its impact on the architectural development of turbidite sheet systems. *Sedimentology*, **58**, 936-959. DOI 10.1111/j.1365-3091.2010.01190.x

Fallgatter, C., Kneller, B., Paim, P.S.G. & Milana, J.P., 2016. Transformation, partitioning and flow-deposit interactions during the run-out of megaflows, *Sedimentology*,**64**, 359-387, doi: 10.1111/sed.12307

Fildes, C.T., 2013. Megabeds: Emplacement Mechanics of Large-Volume Event Beds, PhD thesis, University of Auckland, 256 pp., https://researchspace.auckland. ac.nz/handle/2292/22136

Fildes, C., Stow, D., Riahi, S., Soussi, M., Patel, U., Milton, A.J. & Marsh, S., 2010. European provenance of the Numidian Flysch in northern Tunisia. *Terra Nova*, **22**, 94-102.

Garziglia, S., Sultan N., Cattaneo A., Ker S., Marsset B., Riboulot V., Voisset. M., Adamy, J. & Unterseh, S. 2010. Identification of shear zones and their causal mechanisms using a combination of cone penetration tests and seismic data in the Eastern Niger delta. In: D. Mosher et al. (eds.), Submarine Mass Movements and Their Consequences - *Advances in Natural and Technological Hazards Research*, Springer, **28**, 55-65.

Haughton, P., Davis, C., McCaffrey, W. & Barker, S. 2009. Hybrid sediment gravity flow deposits – Classification, origin and significance. *Marine and Petroleum Geology*, **26**, 1900-1918, doi:10.1016/j.marpetgeo.2009.02.012

Hoogakker, B.A.A., Rothwell, R.G., Rohling, E.J., Paterne, M., Stow, D.A.V., Herrle, J.O. & Clayton, T. 2004. Variations in terrigenous dilution in western Mediterranean Sea pelagic sediments in response to climate change during the last glacial cycle, *Marine Geology,* **211**, 21-43.

Hieke, W., Hirschleber, H.B. & Dehghani, G.A. 2003. The Ionian Abyssal Plain (central Mediterranean Sea): Morphology, subbottom structures and geodynamic history - An inventory. *Marine Geophysical Researches* **24**, 279-310. DOI 10.1007/s11001-004-2173-z

Kastens, K. & Cita, M.B. 1981. Tsunami-induced sediment transport in the abyssal Mediterranean Sea. *Geological Society of America Bulletin,* **92**, 845-857.

Kneller, B., Edwards, D., McCaffrey, W. & Moore, R., 1991, Oblique reflection of turbidity currents, *Geology*, **19**, 250-252, https://doi.org/10.1130/0091-7613(1991)019<0250:OROTC>2.3.CO;2

Mauffret, A., Frizon de Lamotte, D., Lallemant, S., Gorini, C. & Maillard, A. 2004. E–W opening of the Algerian Basin (Western Mediterranean). *Terra Nova*, **16**, 257–264. doi:10.1111/j.1365-3121.2004.00559.x

McHugh, C.M.G., Seeber, L., Cormier, M.-H., Dutton, J., Cagatay, N., Polonia, A., Ryan, W.B.F. & Gorur, N., 2006. Submarine earthquake geology along the North Anatolia fault in the Marmara Sea, Turkey: A model for transform basin sedimentation, *Earth and Planetary Sciences*, **248**, 661-684, doi:10.1016/j.epsl.2006.05.038

McHugh, C.M., Seeber, L., Braudy, N., Cormier, M.-H., Davis, M.B., Diebold, J.B., Dieudonne, N., Douilly, R., Gulick, S.P.S., Hornbach, M.J., Johnson III, H.E., Mishkin, K.R., Sorlien, C.C., Steckler, M.S., Symithe, S.J. & Templeton, J. 2011.

Offshore sedimentary effects of the 12 January 2010 Haiti earthquake. *Geology*, **39**, 723-726, doi:10.1130/G31815.1

Miramontes, E., Garziglia, S., Sultan, N., Jouet, G. & Cattaneo, A. 2018. Morphological control of slope instability in contourites: A geotechnical approach. *Landslides,* **15**, 1085-1095.

Mulder, T., Zaragosi, S., Razin, P., Grelaud, C., Lanfumey, V. & Bavoil, F. 2009. A new conceptual model for the deposition process of homogenite: application to a cretaceous megaturbidite of the western Pyrenees (Basque region, SW France). *Sediment. Geol.*, **222**, 263–273.

Mutti E. 1992. Turbidite Sandstones. AGIP - Istituto di Geologia, Università di Parma, 275 pp .

Polonia, A., Bonatti, E., Camerlenghi, A., Lucchi, R.G., Panieri, G. & Gasperini, L. 2013. Mediterranean megaturbidite triggered by the AD 365 Crete earthquake and tsunami. *Scientific Reports,* **3**, 1285, doi:10.1038/srep01285.

Poort, J. & Lucazeau, F. 2016. WESTMEDFLUX cruise, RV L'Atalante, https://doi.org/10.17600/16000600

Poort, J. & Gorini, C. 2018. WESTMEDFLUX-2 cruise, RV L'Atalante, https://doi.org/10.17600/18000402

Rabineau, M., Droz, L. & Aslanian, D. 2013. AM-MED-1 Cruise, RV Le Suroît, https://doi.org/10.17600/18000821.

Reeder, M.S., Rothwell, R.G. & Stow, D.A.V. 2000. Influence of sea level and basin physiography on emplacement of the late Pleistocene Herodotus Basin Megaturbidite, SE Mediterranean Sea. *Marine and Petroleum Geology*, **17**, 199-218.

Réhault,, J.P., Boillot, G. & Mauffret, A. 1984. The Western Mediterranean Basin geological evolution. *Marine Geology*, **55**, 447-477.

Reimer, P.J., Bard, E., Bayliss, A., Beck, J.W., Blackwell, P.G., Bronk Ramsey, C., Grootes, P.M., Guilderson, T.P., Haflidason, H., Hajdas, I., Hatt, C., Heaton, T.J., Hoffmann, D.L., Hogg, A.G., Hughen, K.A., Kaiser, K.F., Kromer, B., Manning, S.W., Niu, M., Reimer, R.W., Richards, D.A., Scott, E.M., Southon, J.R., Staff, R.A., Turney, C.S.M. & van der Plicht, J. 2013. IntCal13 and Marine13 radiocarbon age calibration curves 0–50,000 years cal BP. *Radiocarbon*, **55**, 1869-1887.

Rothwell, R.G. & Balut, Y. 1995. PALAEOFLUX cruise, RV Marion Dufresne, https://doi.org/10.17600/95200090

Rothwell, R.G., J., T. & Kähler, G. 1998. Low-sea-level emplacement of a very large Late Pleistocene "megaturbidite" in the western Mediterranean Sea. *Nature*, **392**, 377-380.

Rothwell, R.G., Reeder, M.S., Anastasakis, G., Stow, D.A.W., Thomson, J. & Kähler, G. 2000. Lowsea-level stand emplacement of megaturbidites in thewestern and eastern Mediterranean Sea. *Sedimentary Geology*, **135**, 75–88.

Rothwell, R.G., Hoogakker, B., Thomson, J., Croudace, I.W. & Frenz, M. 2006. Turbidite emplacement on the southern Balearic Abyssal Plain (western Mediterranean Sea) during Marine Isotope Stages 1-3: an application of ITRAX XRF scanning of sediment cores to lithostratigraphic analysis. In: Rothwell, R.G., (ed.) New techniques in sediment core analysis. London, UK, Geological Society of London, 79-98, 266 pp. (Geological Society Special Publication, 267).

SanPedro, L., Babonneau, N., Gutscher, M.A. & Cattaneo, A. 2017. Origin and chronology of the Augias deposit in the Ionian Sea (Central Mediterranean Sea), based on new regional sedimentological data. *Marine Geology*, **384**, 199-213.

Stanley, D.J., McCoy, F.W. & Diester-Haass, L. 1974. Balearic abyssal plain: an example of modern basin plain deformation by salt tectonism. *Marine Geology*, **17**, 183-200.

Stow,D., Fildes, C., Riahi, S., Soussi, M., Patel, U., Milton, J.A. &Marsh, S. 2010. Reply to comment on 'European provenance of the Numidian Flysch in northern Tunisia'. *Terra Nova*, **22**, 504-505, doi: 10.1111/j.1365-3121.2010.00966.x

Sultan, N. 2007. PRISME cruise, RV L'Atalante, https://doi.org/10.17600/7010090

Talling, P.J. 2013. Hybrid submarine flows comprising turbidity current and cohesive debris flow: Deposits, theoretical and experimental analyses, and generalized models. *Geosphere*, **9**. 460-488. https://doi.org/10.1130/GES00793.1A

Talling, P.J., Clare, M., URlaub, M., Pope, E., Hunt, J.E. & Watt, S.F.L. 2014. Large submarine landslides on continental slopes slopes: Geohazards, methane release, and climate change. *Oceanography,* **27**, 32-45, http://dx.doi.org/10.5670/oceanog.2014.38.

Thomas, M.F.H., Bodin, S., Redfern, J. & Irving, D.H.B. 2010. A constrained. African craton source for the Cenozoic Numidian Flysch: implications for the palaeogeography of the western Mediterranean basin. *Earth Sci. Rev*., **101**, 1-23.

Vigliotti, L. 2008. Comment on ''Lost tsunami'' by Maria Teresa Pareschi et al. *Geophysical Research Letters*, **35**, L02608, doi:10.1029/2007GL031155

Zuffa, G.G., Normark, W.R., Serra, F. & Brunner, C.A. 2000. Turbidite megabeds in an oceanic rift valley recording jökulhlaups of late Pleistocene glacial lakes of the western United States. *J. Geol*., **108**, 253-274.

Zúñiga, D., García-Orellana, J., Calafat, A., Price, N.B., Adatte, T., Sanchez-Vidal, A., Canals M., Sanchez-Cabeza J.A., Masqué, P. & Fabres, J. 2007. Late Holocene fine-grained sediments of the Balearic Abyssal Plain, Western Mediterranean Sea. *Marine Geology*, **237**, 25-36.

Table and Figure captions

Tab. 1. Sediment cores in the Balearic abyssal plain with entire or partial recovery of the megabed with indication of the coordinates, water depth, basin sector, distribution of sediment facies within the megabed, and reference. BAP = Balearic Abyssal Plain. Cores MD81 come from campaign PALEOFLUX (Rothwell and Balut, 1995), cores PSM from campaign PRISME (Sultan, 2007), cores WMF and WFM2 from campaigns WestMedFlux (Poort and Lucazeau, 2016) and WestMedFlux2 (Poort and Gorini, 2018).

Tab. 2. List of radiocarbon ages. Lab code “Poz” indicates measurements done by Poznan Radiocarbon Laboratory (Poland), while “Beta” is for Beta Analytic.. Age min and age max correspond to the calibrated ages 2σ (CAL BP) calculated by CALIB program with the calibration curve Marine 13 (Reimer et al., 2013), with a reservoir age of 400 yr.

Fig. 1. General bathymetric map of the Balearic abyssal plain (BAP) with location of seismic surveys (colour lines, see the graphic legend to identify the name of the cruise) and sediment cores (red dots) mentioned or presented in this study. The continuous black line represent the indicative areal coverage of the BAP megabed as proposed by Rothwell et al. (2000). White boxes show the location of seismic profiles presented in Figures 2, 3, 5 and 6. The dashed black line shows a proposed extent of the megabed based on sediment core evidence from Babonneau et al. (2017) and this study.

Fig. 2. Sub-Bottom Profiles from campaigns WestMedFlux (2016) with images of the BAP megabed identifiable as an acoustically transparent layer. (a) Profile WMF2016-AT010_T120939 shows the acoustically transparent unit of the BAP megabed less thant 10 m below the seafloor with gentle folds following the geometry of underlying strata and a gradual pinch-out of the unit towards the SouthWest. (b) Profile WMF2016-AT010_T215750 shows in the central part of the basin the presence of faults displacing the megabed.

Fig. 3. (a) Profile WMF2018-AT141A with evidence of the pinch-out of the BAP megabed towards the west beyond salt domes. The lateral termination of the megabed seems to be at offset 15000, but it actually goes further west (offset 1000). (b) Profile SARDINIA2006209 with abrupt eastward termination of the BAP megabed on the steep Sardinian margin testified by diffraction hyperbolae and thickness variability due to the presence of salt domes towards NW. (c) Profile SARDINIA2006172 with a detail of the abrupt eastward termination against the Sardinia margin.

Fig. 4. SBP profile WMF2018-AT143A in a sector where the BAP megabed is relatively isopach by folded by salt diapirs and cut by vertical faults showing metric displacement (a). The pop-up image (b) shows evidence of erosion at the base of the BAP megabed with apparent truncation of seismic reflectors.(c) Map with location of the seismic profile. The dashed blue line shows the area with occurrence of seismic reflector truncations at the base of the megabed.

Fig. 5. (a) Profile WMF2016-AT012 where the BAP megabed is dissected by several vertical faults (location in **Fig. 1**). (b) The pop-up image shows three distinct echo-facies within the BAP megabed: I faint discontinous and very low amplitude reflectors echo-facies, II dominantly transparent echo-facies topped by a discontinuous but mappable reflector, III basal unit with a discontinuous base and top showing medium-amplitude discontinuous reflectors. (c) Legend of the echo-facies.

Fig. 6. (a) Portion of SBP profile WMF2016-AT016 at the site of sediment core WMF2-KF11 (Location in **Fig. 1**). (b, d) Core WMF2-KF11 photo. Note the 4 intervals in blue where whole core samples for oedometer tests were reserved: two within the homogeneous clay of the megabed, two in overlying layers characterised by alternating thin beds of sand and silt with dominant hemipelagic silty clay (the latter two samples are from fine grained sediment). (c) P-wave velocity log of the core showing a clear identification of three lithological units.

Fig. 7. (a) Lithological log of sediment cores LC05 (only the upper ca. 13 m, modified from Clare et al., 2014) and WMF2-KF11. Note that the majority of the sedimentary succession is represented by turbidites. (b) Synthetic sedimentary structures of the megabed. (c) Map showing the possible sources of the megabed (arrows, modified

from Clare et al., 2014), thickness value of the megabed (from **Tab. 1**) and earthquake epicentres of Mw>2 from the ESMC Catalogue http://www.emsc-csem.org.

Fig. 8. Transect of sediment cores PSM3-KS21, -KS23 and -KS27 offshore the Algerian margin. Only the upper part of the cores is visible, see the whole correlation in Babonneau et al. (2017 ; their Fig. 7). Note in the grey shaded area a sediment layer standing out in photos for its colour different from that of other encasing turbidity layers whose age is compatible with that of the BAP megabed (**Tab. 2**). Core identifier are: PSM-KS21 (http://igsn.org/BFBGX-86346); PSM-KS23: http://igsn.org/BFBGX-86348; PSM-KS27 : http://igsn.org/BFBGX-86352.

Fig. 9 S Physical and geotechnical parameters measured on core WMF2-KF11. From left to right: Density form Multi Sensor Core Logger (MSCL, black line) and from water content on discrete samples (blue dots); P-wave velocity from MSCL (black line) and discrete measurements on half core via celerimeter (blue dots); Derived parameters from oedometric tests Yield Stress Ratios (YSR) and Recompression, Compression and Swelling Indices; Undrained shear strength (Su) measured by Vane test in the half core: normally consolidated sediment would fall within the black and red lines. Note the abrupt change of several parameters at 2.28 mbsf. The grey shadow correspond to the depth of the homogenite part of the BAP megabed (2.28-4.50 mbsf), whereas in yellow is the silty/sandy portion of the megabed sampled by the core.

Core Name	Lat N (DDMM.xx)	Lon E (DDMM.xx)	w. depth m	Location within the BAP	Megabed sampled (Y/N)	Top megabed (clay) (mbsf)	Top silt of megabed (mbsf)	Top sand of megabed (mbsf)	Base megabed (mbsf)	Total megabed thickness (m)
MD81-LC01	40° 15.82'	6°53.23'	2845	Abyssal Plain	Y	14.5	19.7	21.8	22.8	8.3
MD81-LC02	39°31.88	6°22.58	2860	Abyssal Plain	Y	8.7	15	/	16.4	7.7
MD81-LC04	38°39.01	6°06.64	2855	Abyssal Plain	Y	6.2	14.4	/	16.8	10.6
MD81-LC05	38°00.92	5°29.95	2845	Abyssal Plain	Y	6	10.2	10.9	11.4	5.4
MD81-LC06	38°00.66	7°11.09	2845	Abyssal Plain	Y	14.5	19.0	19.2	20.2	5.7
PSM-KS21	37° 09.953′	2° 42.127′	2779	Algerian Margin	Y	8.8	/	/	8.9	0.1
PSM-KS23	37° 27.093′	2° 59,526′	2775	Algerian Margin	Y	4.9	/	/	5.2	0.3
PSM-KS27	37° 18.102	3° 24.317′	2791	Algerian Margin	Y	10.5	/	/	11.5	1
WMF2-KF02	38°56.766'	5°32.448'	2848	E of Minorca	Y	4.6	?	?	>6.99	>2.39
WMF2-KF11	39°37.168'	6°9.609’	2848	E of Minorca	Y	2.28	?	?	>5.92	>3.64
WMF-KF10	37°52.797'	2°20.883'	2795	S of Minorca	?	3.9?	?	?	4.3	maybe 0.4
WMF-KF11	37°49.109'	2°23.578'	2796	S of Minorca	?	3?	?	?	3.8	maybe 0.8

Tab. 1.

Core	Sample interval (cm)	Foram. species	Lab code	Age ^{14}C	Error +/-	Age min CAL BP	Age max CAL BP	Source
PSM-KS21	837-838	*G. ruber*	Poz-68081	16790	90	19383	19881	Babonneau et al., 2017
PSM-KS23	423-424.5	*G. ruber*	Poz-68119	15270	80	17806	18521	Babonneau et al., 2017
WMF2-KF11	1.51-1.52	*G. bulloides*	Beta-508507	10530	30	11250	12031	This study
WMF2-KF11	2.02-2.03	*G. bulloides*	Beta-508508	14450	50	16595	17385	This study
WMF2-KF11	2.10-2.11	*G. bulloides*	Beta-508509	17030	60	19652	20325	This study

Tab. 2.

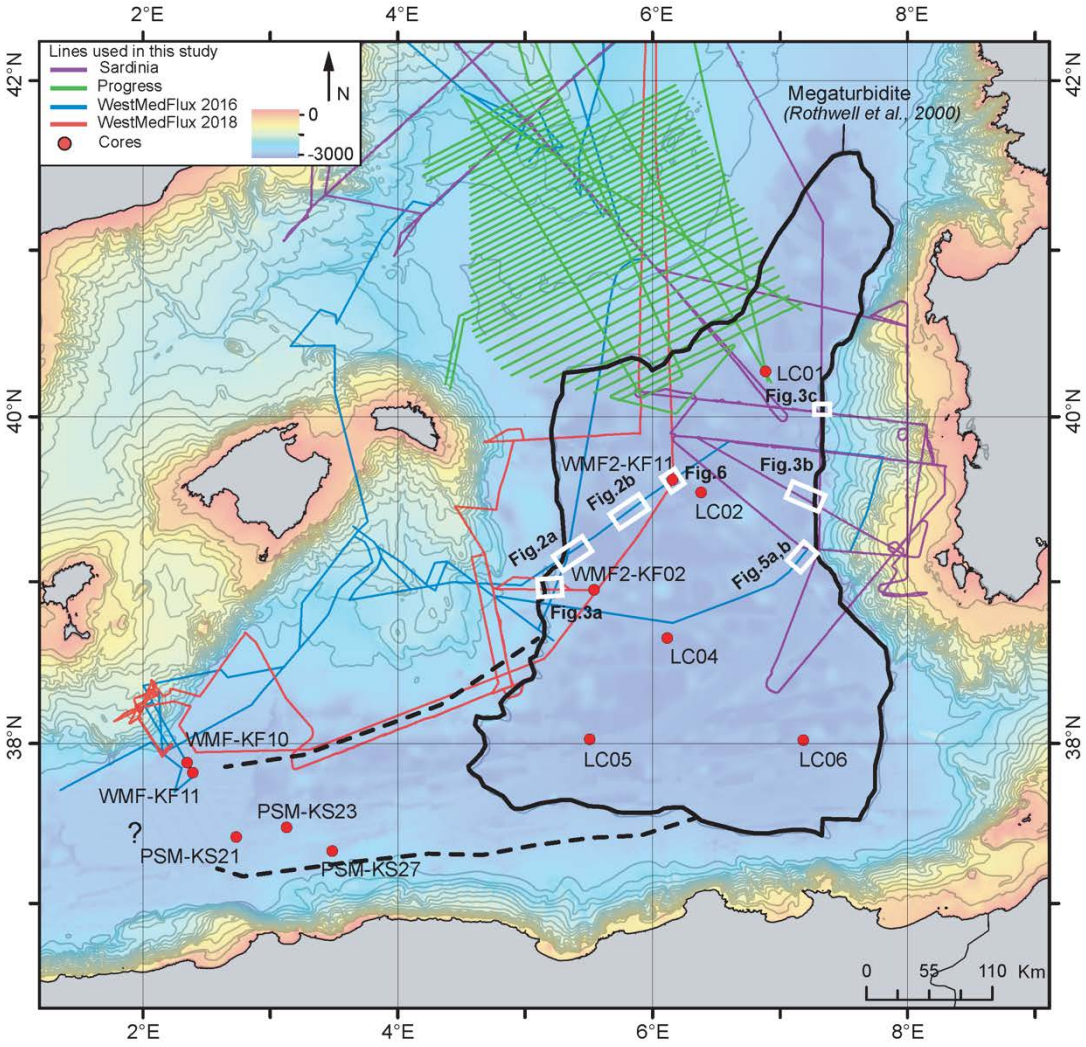
Lines used in this study
Sardinia
Progress
WestMedFlux 2016
WestMedFlux 2018
Cores
N
0
-3000
Megaturbidite
(Rothwell et al., 2000)
LC01
Fig.3c
WMF2-KF11
Fig.6
Fig.3b
Fig.2b
LC02
Fig.2a
WMF2-KF02
Fig.5a,b
Fig.3a
LC04
WMF-KF10
LC05
LC06
WMF-KF11
PSM-KS23
?
PSM-KS21
PSM-KS27
0 55 110 Km
2°E
4°E
6°E
8°E
42°N
40°N
38°N

Fig. 1

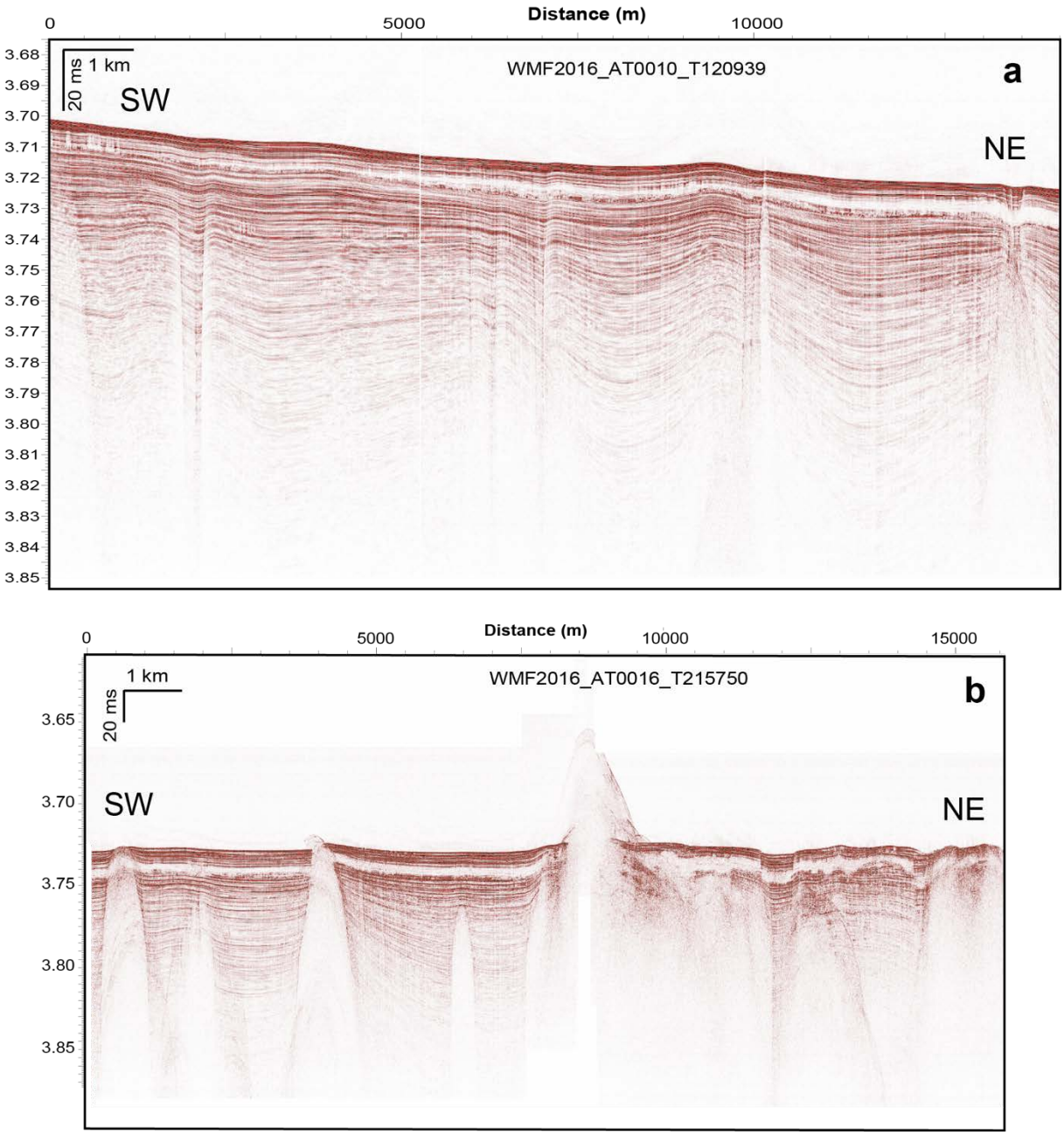
Distance (m)
0
5000
10000
15000
3.68
3.69
3.70
3.71
3.72
3.73
3.74
3.75
3.76
3.77
3.78
3.79
3.80
3.81
3.82
3.83
3.84
3.85
20 ms
1 km
SW
NE
WMF2016_AT0010_T120939
a
WMF2016_AT0016_T215750
b
3.65
3.70
3.75
3.80
3.85

Fig. 2

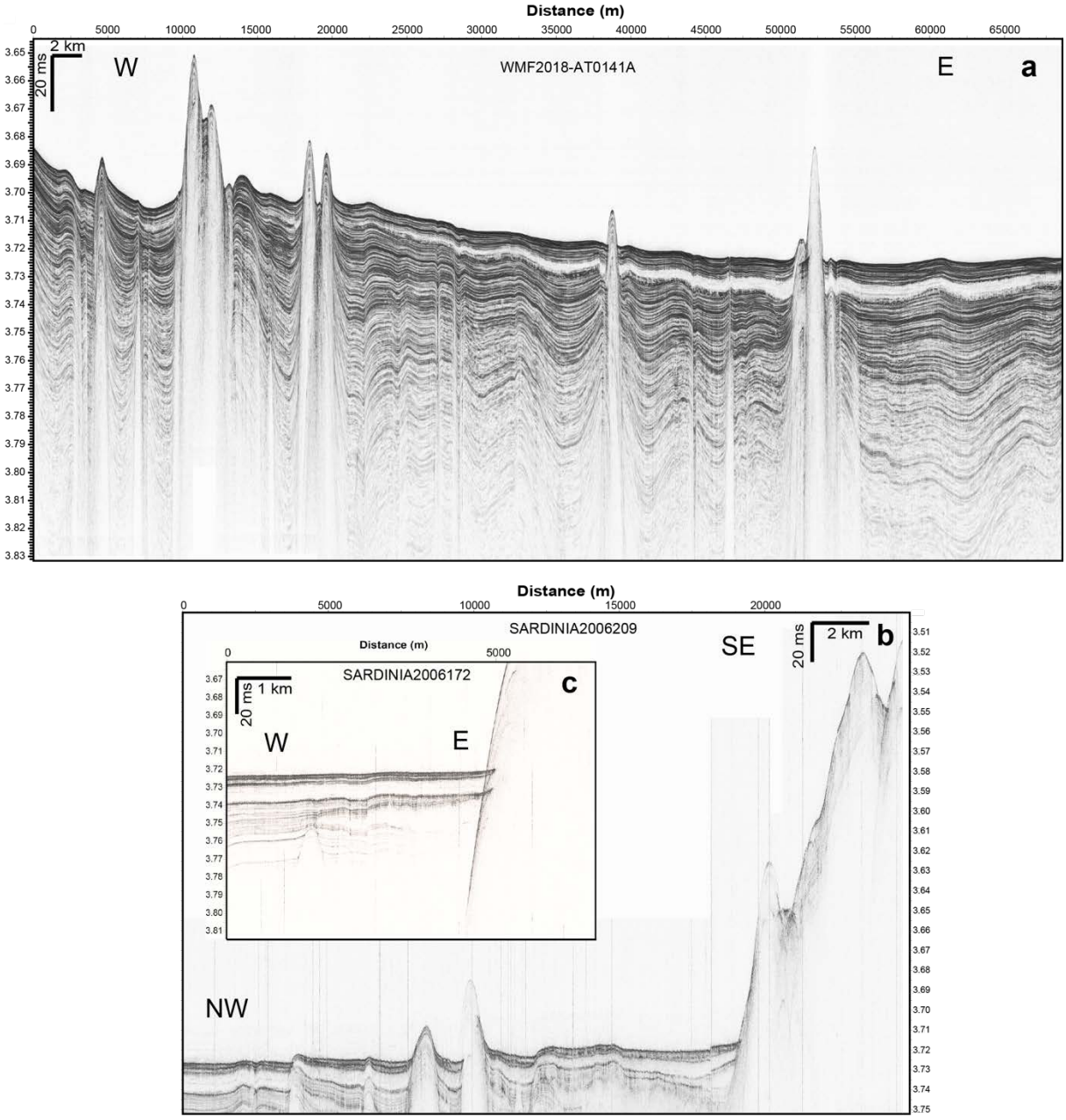
Distance (m)
0
5000
10000
15000
20000
25000
30000
35000
40000
45000
50000
55000
60000
65000
2 km
20 ms
W
WMF2018-AT0141A
E
a
Distance (m)
0
5000
10000
15000
20000
SARDINIA2006209
SE
20 ms
2 km
b
Distance (m)
0
5000
SARDINIA2006172
20 ms
1 km
c
W
E
NW

Fig. 3

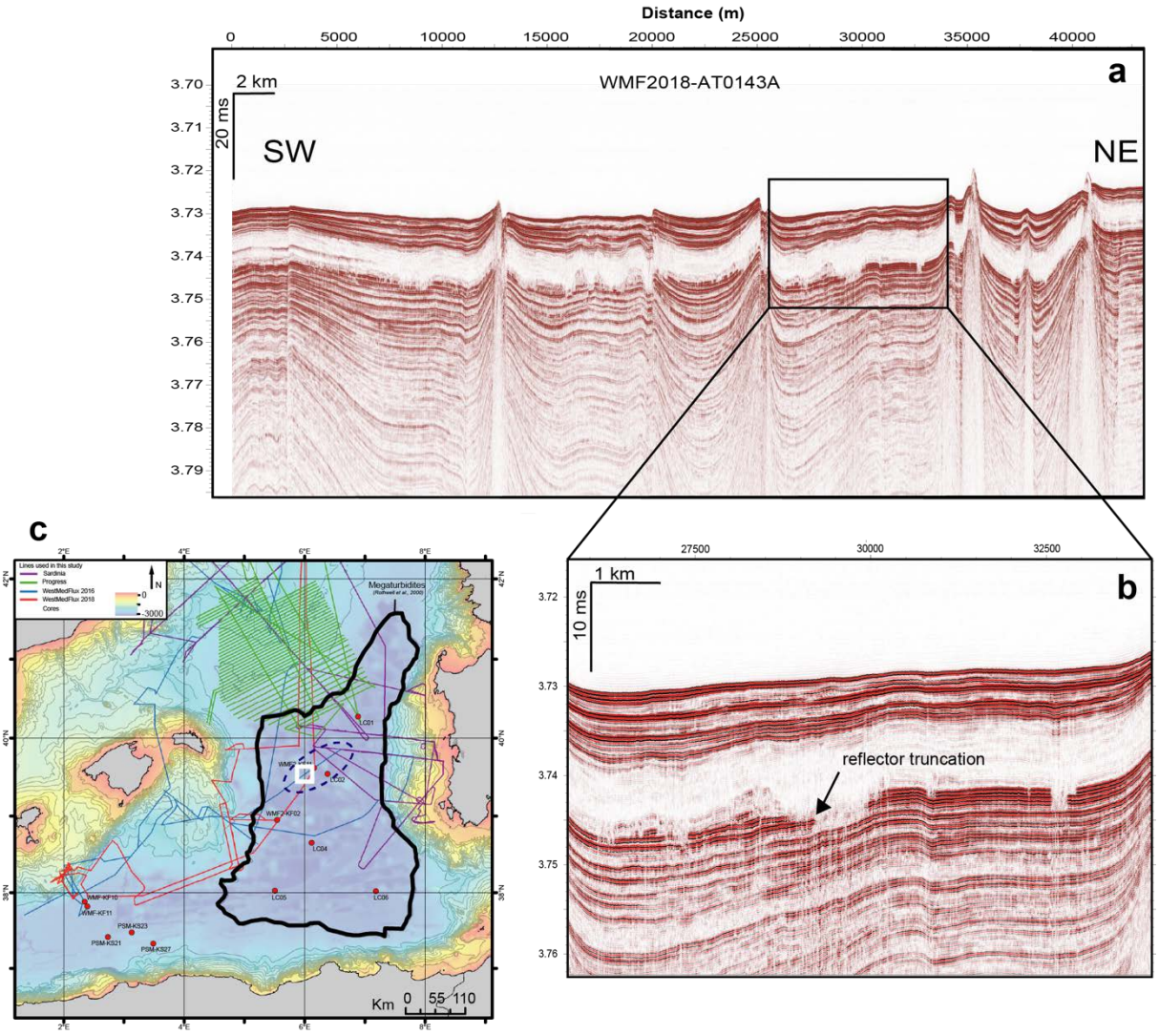
Distance (m)
0
5000
10000
15000
20000
25000
30000
35000
40000
a
WMF2018-AT0143A
2 km
20 ms
SW
NE
3.70
3.71
3.72
3.73
3.74
3.75
3.76
3.77
3.78
3.79
b
1 km
10 ms
27500
30000
32500
reflector truncation
c
Megaturbidites
Km
0
55
110

Fig. 4

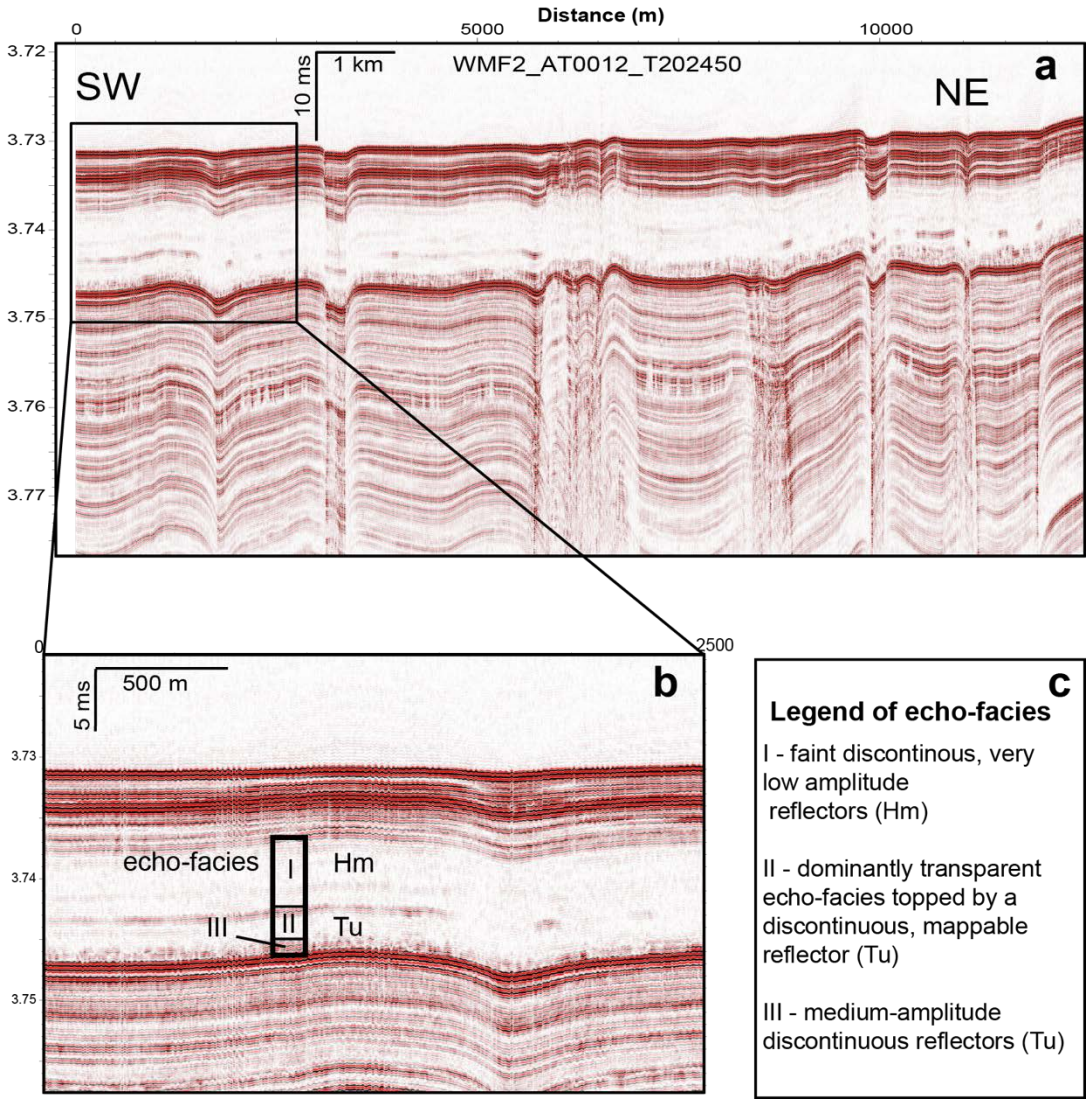
Distance (m)
0
5000
10000
SW
NE
a
1 km
10 ms
WMF2_AT0012_T202450
3.72
3.73
3.74
3.75
3.76
3.77
0
2500
b
500 m
5 ms
echo-facies
I
Hm
II
Tu
III
c
Legend of echo-facies
I - faint discontinous, very low amplitude reflectors (Hm)
II - dominantly transparent echo-facies topped by a discontinuous, mappable reflector (Tu)
III - medium-amplitude discontinuous reflectors (Tu)

Fig. 5

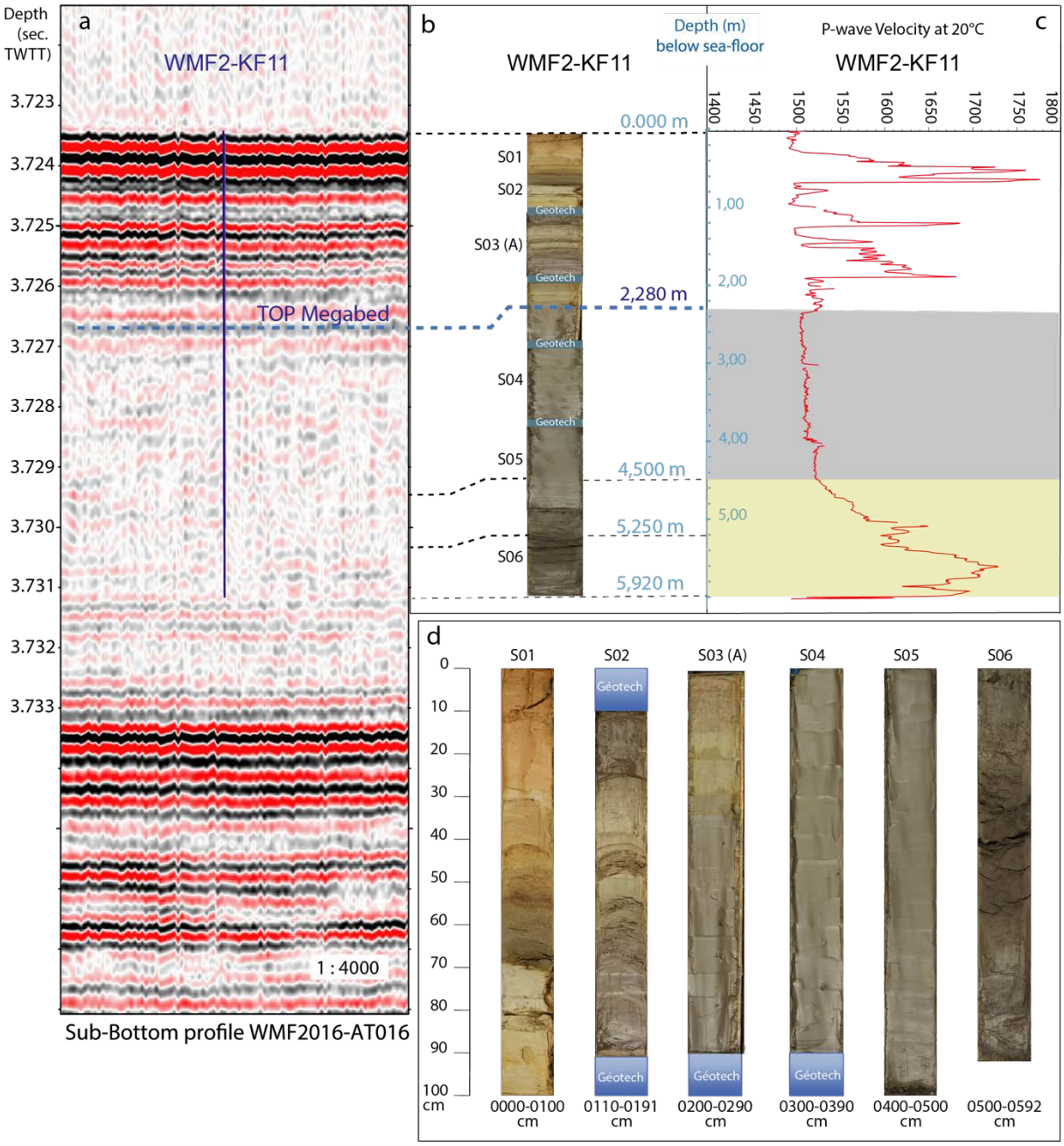
a
Depth (sec. TWTT)
WMF2-KF11
3.723
3.724
3.725
3.726
3.727
3.728
3.729
3.730
3.731
3.732
3.733
TOP Megabed
1 : 4000
Sub-Bottom profile WMF2016-AT016
b
WMF2-KF11
Depth (m) below sea-floor
0.000 m
S01
S02
Geotech
S03 (A)
Geotech
2,280 m
Geotech
S04
Geotech
S05
4,500 m
5,250 m
S06
5,920 m
c
P-wave Velocity at 20°C
WMF2-KF11
1400
1450
1500
1550
1600
1650
1700
1750
1800
1,00
2,00
3,00
4,00
5,00
d
S01
S02
S03 (A)
S04
S05
S06
0
10
20
30
40
50
60
70
80
90
100
cm
Géotech
Géotech
Géotech
Géotech
0000-0100 cm
0110-0191 cm
0200-0290 cm
0300-0390 cm
0400-0500 cm
0500-0592 cm

Fig. 6

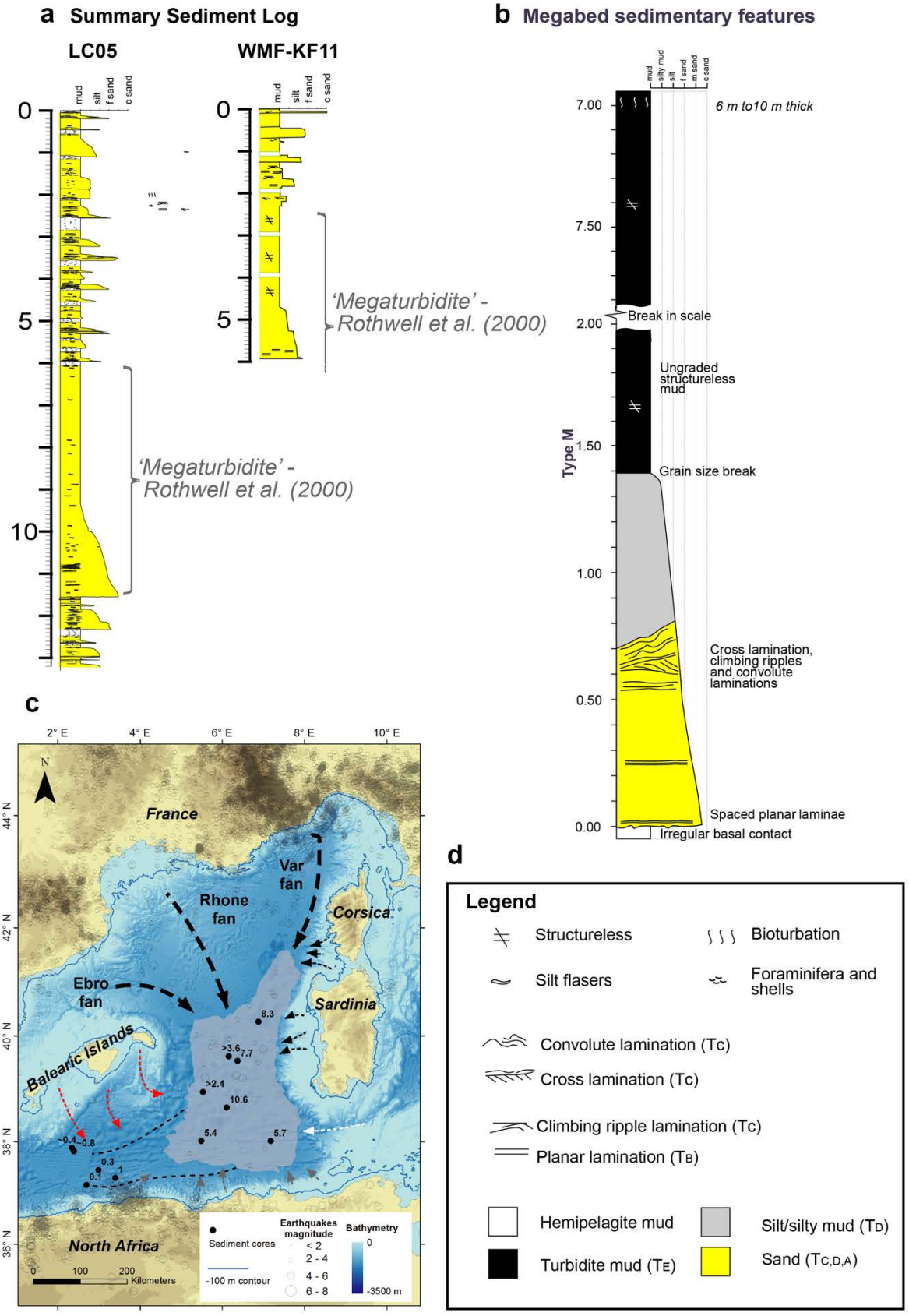
a Summary Sediment Log
LC05
WMF-KF11
mud
silt
f sand
c sand
0
5
10
'Megaturbidite' - Rothwell et al. (2000)
'Megaturbidite' - Rothwell et al. (2000)
b Megabed sedimentary features
mud
silty mud
silt
f sand
m sand
c sand
7.00
7.50
2.00
1.50
1.00
0.50
0.00
Type M
6 m to10 m thick
Break in scale
Ungraded structureless mud
Grain size break
Cross lamination, climbing ripples and convolute laminations
Spaced planar laminae
Irregular basal contact
c
2° E
4° E
6° E
8° E
10° E
44° N
42° N
40° N
38° N
36° N
N
France
Var fan
Rhone fan
Corsica
Ebro fan
Sardinia
Balearic Islands
North Africa
8.3
>3.6
7.7
>2.4
10.6
5.4
5.7
~0.4
0.8
0.3
1
0.1
Sediment cores
-100 m contour
Earthquakes magnitude
< 2
2 - 4
4 - 6
6 - 8
Bathymetry
0
-3500 m
0
100
200
Kilometers
d
Legend
Structureless
Bioturbation
Silt flasers
Foraminifera and shells
Convolute lamination (Tc)
Cross lamination (Tc)
Climbing ripple lamination (Tc)
Planar lamination (TB)
Hemipelagite mud
Silt/silty mud (TD)
Turbidite mud (TE)
Sand (TC,D,A)

Fig. 7

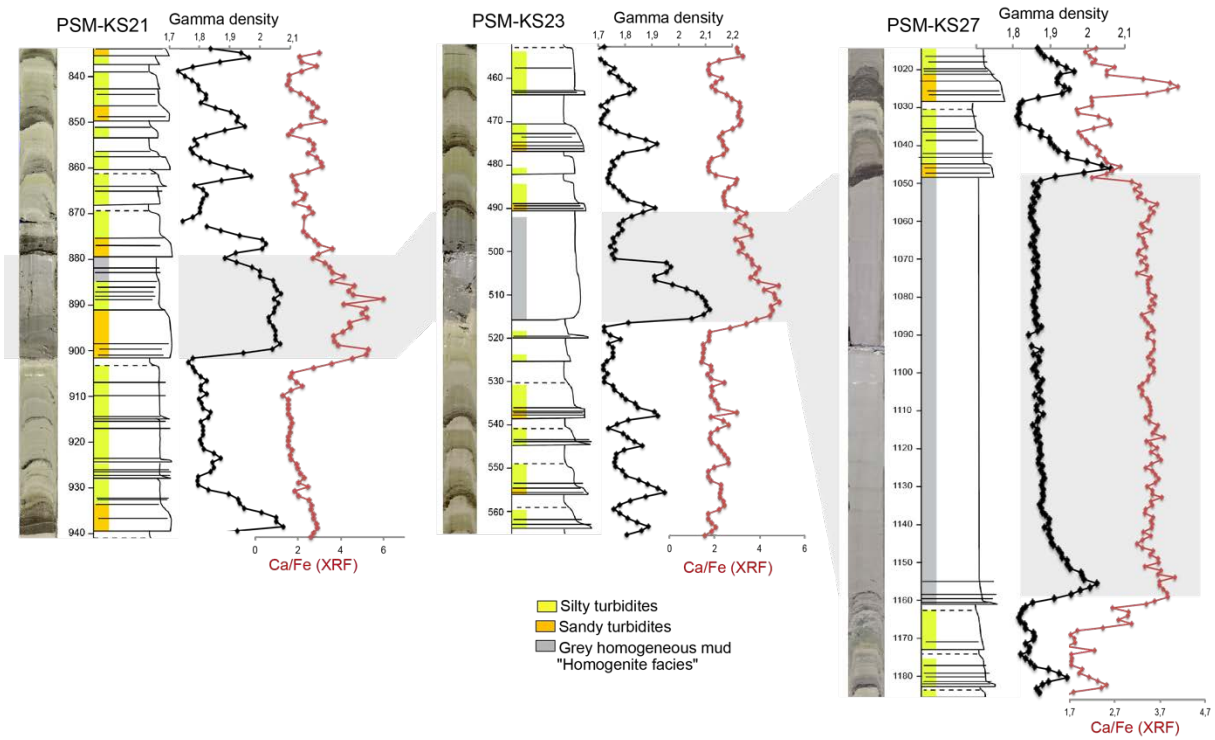
PSM-KS21
Gamma density
1,7 1,8 1,9 2 2,1
840
850
860
870
880
890
900
910
920
930
940
0 2 4 6
Ca/Fe (XRF)
PSM-KS23
Gamma density
1,7 1,8 1,9 2 2,1 2,2
460
470
480
490
500
510
520
530
540
550
560
0 2 4 6
Ca/Fe (XRF)
PSM-KS27
Gamma density
1,8 1,9 2 2,1
1020
1030
1040
1050
1060
1070
1080
1090
1100
1110
1120
1130
1140
1150
1160
1170
1180
1,7 2,7 3,7 4,7
Ca/Fe (XRF)
Silty turbidites
Sandy turbidites
Grey homogeneous mud
"Homogenite facies"

Fig. 8

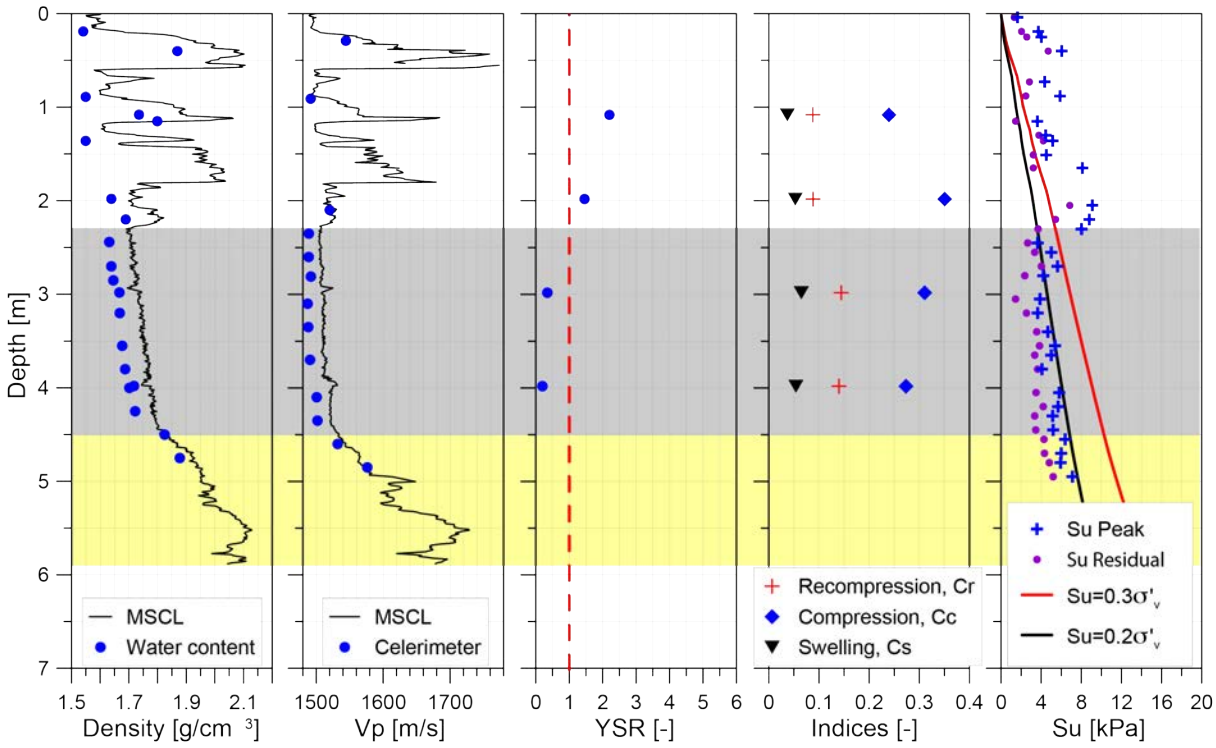
Depth [m]
0
1
2
3
4
5
6
7
MSCL
Water content
Density [g/cm 3]
1.5 1.7 1.9 2.1
MSCL
Celerimeter
Vp [m/s]
1500 1600 1700
YSR [-]
0 1 2 3 4 5 6
Recompression, Cr
Compression, Cc
Swelling, Cs
Indices [-]
0 0.1 0.2 0.3 0.4
Su Peak
Su Residual
Su=0.3σ'v
Su=0.2σ'v
Su [kPa]
0 4 8 12 16 20

Fig. 9